Ann. Chim. Sci. Mat., 2002, 27 (6), pp. 15-36

HYDROTHERMAL CRYSTALLIZATION OF CERAMICS

Richard E. RIMAN[a], Wojciech L. SUCHANEK[b], and Malgorzata M. LENCKA[c]

[a] Rutgers University, Department of Ceramic and Materials Engineering, 607 Taylor Road, Piscataway, New Jersey 08854-8065, USA.
[b] Sawyer Research Products, Inc., 35400 Lakeland Blvd., Eastlake, Ohio 44095, USA.
[c] OLI Systems, Inc., 108 American Road, Morris Plains, New Jersey 07950, USA.

Abstract - In broad terms, hydrothermal synthesis is a technology for crystallizing materials (chemical compounds) directly from aqueous solution by adept control of thermodynamic variables (*temperature, pressure and composition*). The objective of this chapter is to introduce the field of hydrothermal materials synthesis and show how understanding solution thermodynamics of the aqueous medium can be used for engineering hydrothermal crystallization processes. In the first section, we will focus on hydrothermal synthesis as a materials synthesis technology by providing history, process definitions, technological merits and comments on its current implementation in industry. In the second section, we will describe how thermodynamic modeling is being developed as an engineering tool to predict equilibrium phase assemblages and use this predictive power as an engineering tool for development of hydrothermal technology for materials synthesis.

Résumé – Cristallisation hydrothermale de ceramiques. De manière générale, la synthèse hydrothermale est une technologie pour la cristallisation de matériaux (composés chimiques), directement à partir d'une solution aqueuse, et grâce à un contrôle approprié des variables thermodynamiques (température, pression et composition). L'objectif de ce chapitre est d'introduire le domaine de la synthèse hydrothermale des matériaux et de montrer comment la compréhension de la thermodynamique des milieux aqueux peut être mise à profit dans l'ingénierie des procédés de cristallisation hydrothermale. Dans la première partie, nous nous concentrerons sur la synthèse hydrothermale en tant que technologie de synthèse de matériaux en donnant des éléments historiques, les définitions du procédé, les avantages et inconvenients technologiques ainsi que des commentaires sur sa mise en application en milieu industriel. Dans la deuxième partie, nous décrirons comment la modélisation thermodynamique sert d'outil d'ingénierie pour prédire les assemblages de phases à l'équilibre, et comment utiliser cette puissance de prédiction pour le développement de la technologie hydrothermale appliquée à la synthèse de matériaux.

Reprints : R. E. Riman, Rutgers University, Department of Ceramic and Materials Engineering, 607 Taylor Road, Piscataway, New Jersey 08854-8065, USA.

1. HYDROTHERMAL SYNTHESIS AS A MATERIALS SYNTHESIS TECHNOLOGY

1.1. Brief history

The first publications on hydrothermal synthesis of ceramics started appearing in the scientific literature in the middle of the 19th century [1]. Hydrothermal research was conducted by geologists and was aimed at simulating natural hydrothermal phenomena occurring in the Earth's crust in the laboratory, which helped to better understand geological processes. Progress in synthesis was accelerated by significant developments in hydrothermal pressure vessel engineering. While the 19th century confined hydrothermal research mostly to Germany, France, Italy, and Switzerland, the 20th century brought in the USA, the Soviet Union, and Japan as major centers for development of hydrothermal technology. With respect to this chapter, the 20th century is the period when hydrothermal synthesis was clearly identified as an important technology for materials synthesis, predominantly in the field of single crystal growth [2]. However, the severe (supercritical) reaction conditions required for growing single crystals have discouraged extensive commercialization for many materials. For example, hydrothermal epitaxy was very popular during the 1970s, however, it did not achieve commercial success due to the high temperatures and pressures involved (T>500°C, P>100 MPa) [3]. In recent years, commercial interest in hydrothermal synthesis has been revived in part because a steadily increasingly large family of materials has emerged that can be prepared under mild conditions (T<350°C, P<100 MPa). The growing number of scientific papers, which almost tripled between 1989 and 1999, illustrates the rising interest in hydrothermal synthesis. During this period, the United States, Japan, and China contributed 55% of all the papers on hydrothermal processing in materials science published in the world, with the USA (23%) leading ahead of Japan (19%) [4].

1.2. Hydrothermal synthesis: a process definition

Hydrothermal synthesis is a process that utilizes single or heterogeneous phase reactions in aqueous media at elevated temperature (T>25°C) and pressure (P>100 kPa) to crystallize anhydrous ceramic materials directly from solution. However, researchers also use this term to describe processes conducted at ambient conditions. Syntheses are usually conducted at autogeneous pressure, which corresponds to the vapor pressure above the solution at the specified temperature and composition of the hydrothermal solution. However, in the case of hydrothermal growth of single crystals, additional pressure adjustment is done to control solubility and growth rate [5, 6]. Reactants used in hydrothermal synthesis are generally called precursors, which are administered in the form of solutions, gels, and suspensions. Mineralizers are either inorganic or organic additives that are often used to control pH but are used at excessively high concentrations (e.g., 10 m) to also promote solubility. Other additives, also organic or inorganic, are used to serve other functions such as promote particle dispersion or control crystal morphology.

Upper limits of hydrothermal synthesis extend to over 1000°C and 500 MPa pressure [7]. Nevertheless, from the point of view of large-scale materials production, practical temperature and pressure restrictions fall around 350°C and 100 MPa (saturated vapor pressure of water at this temperature is ≈16 MPa) below which reaction conditions are considered mild and above which conditions are considered severe. This transition from mild to severe conditions is determined mostly by corrosion and strength limits of the materials of construction that comprise the hydrothermal reaction vessels. Intensive research has led to a better understanding of the hydrothermal chemistry, which has significantly reduced the reaction time, temperature, and pressure for hydrothermal crystallization of materials. A significant number of chemical systems in

the form of powders and films can be synthesized in the range between that of ambient conditions and temperatures and pressures of 200°C and < 1.5 MPa, respectively. This breakthrough has made hydrothermal synthesis more economical since processes can be engineered using cost-effective and proven pressure reactor technology and methodologies already established by the chemical process industry. In addition, the maintenance and safety procedures are far less involved with reactions performed under mild conditions as opposed to severe ones, which are considerations that influence productivity and cost. Thus, problems relating to scale-up issues are more easily addressed than in other emerging advanced technologies (e.g., molecular beam epitaxy).

Hydrothermal synthesis can be distinguished from solvothermal synthesis methods [8] and "soft solution processing" [4]. Solvothermal synthesis utilizes non-aqueous solvents instead of an aqueous medium [8]. For example, glycothermal synthesis is a solvothermal method that utilizes glycols solvents such as ethylene glycol or 1,4-butanediol. "Soft solution processing" is a broad term that encompasses many well-established, processing routes that utilize mild reaction conditions, which include hydrothermal synthesis among other methods such as bio-mimetic processing, electro-deposition, self-assembly, etc.

A variety of materials have been synthesized by hydrothermal methods, such as stabilized zirconia [9], $BaTiO_3$ [10], $Pb(Zr_xTi_{1-x})O_3$ [11], hydroxyapatite [12], quartz [5], zeolites [13], vanadates [14], and phosphates [2]. It appears that the hydrothermal technique is well suited not only for fabrication of simple and complex oxides, but also for non-oxide materials, such as fluorides, sulfides, and pure elements. For example, various forms of carbon, such as diamond [15] and multi-walled carbon nanotubes [16] can be fabricated under hydrothermal conditions.

1.3. The merits of hydrothermal synthesis

Hydrothermal synthesis offers many advantages over conventional and non-conventional ceramic synthetic methods. All forms of ceramics can be prepared with hydrothermal synthesis, namely powders, fibers, and single crystals, monolithic ceramic bodies, and coatings on metals, polymers, and ceramics. Unlike many advanced methods that can prepare a large variety of forms, such as chemical vapor-based methods, the respective costs for instrumentation, energy and precursors are far less for hydrothermal methods. From the environmental perspective, hydrothermal methods are more environmentally benign than many other synthesis methods. This can be attributed in part to energy conservant low processing temperatures, ability to recycle waste, and safe and convenient disposal of waste that cannot be recycled. The low reaction temperatures also avoid other problems encountered with high temperature processes such as poor stoichiometry control due to volatilization of components (e.g., lead volatilization in lead-based ceramics) and stress-induced defects (e.g., micro-cracks) caused by phase transformations that occur as the ceramic is cooled to room temperature. From the standpoint of ceramic powder production, there are far fewer time- and energy-consuming processing steps since mixing and milling steps are not necessary. Moreover, the ability to precipitate the powders directly from solution regulates the rate and uniformity of nucleation, growth and aging, which affords size, morphology and aggregation control that is not possible with many synthesis processes [17, 18]. *Figure 1* shows several examples of the varieties of morphologies and particle sizes possible with hydrothermal processing. In the future, many industries that rely on powder (e.g., materials, pigments, pharmaceuticals, medical diagnostics) will benefit from having access to powders with controlled size and morphology for a wide range of reasons beyond the scope of this chapter. For instance, in the materials community, the elimination of aggregates leads to optimized and reproducible properties because of better microstructure control [19, 20]. From the standpoint of thin films (coatings), other methods such as physical vapor deposition, chemical vapor deposition and sol-gel suffer from the

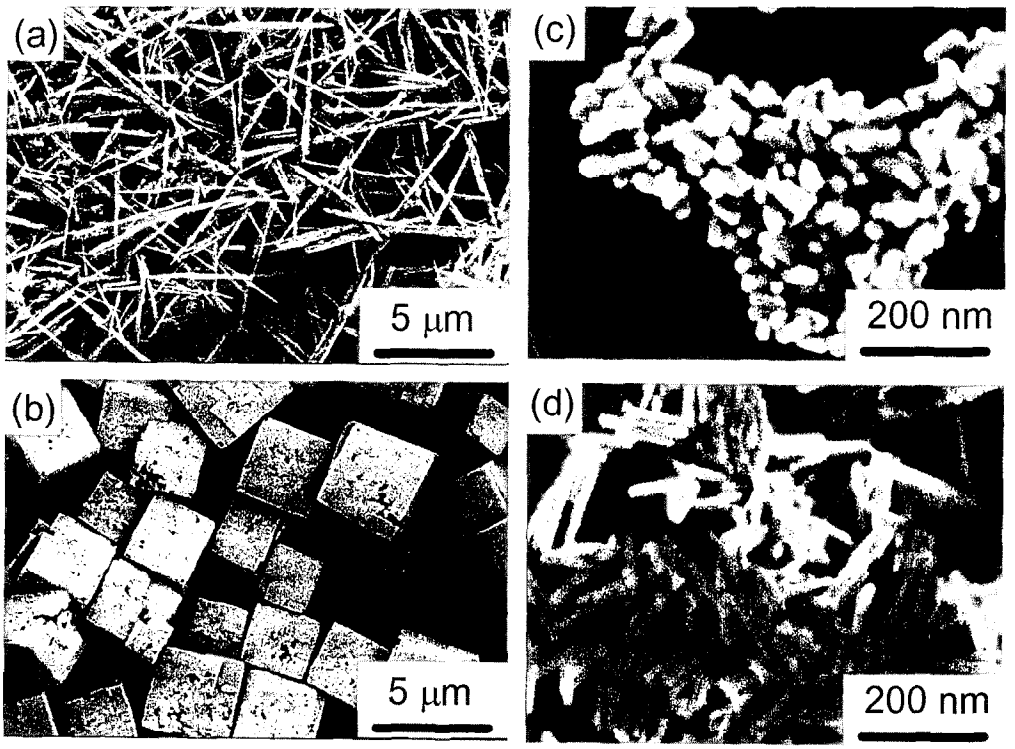

Figure 1. (a) and (b) PZT crystals prepared hydrothermally at 150°C for 24 h at moderate stirring. In both cases, Pb-acetate and Zr-Ti-hydrous oxide were used as sources of Pb, Zr, and Ti, respectively. Total concentration of (Zr+Ti) was 0.1 m and the Pb:Zr:Ti ratio was 1.1:0.52:0.48. Concentration of the TMAH mineralizer was (a) 0.5 m, (b) 1.0 m. (c) and (d) Hydroxyapatite crystals prepared hydrothermally at 200°C for 24 h at pH=10.0 at moderate stirring. (c) Powders crystallized in 50 vol. % 2-propanol (aq). (d) Powders crystallized in 1 wt.% KCl (aq).

disadvantage that they all require high temperature processing to crystallize the ceramic phase. Thermally induced defects result, such as cracking, peeling, undesired reactions between the substrate and coating and decomposition of the substrate material. In contrast, hydrothermal synthesis can be used to directly crystallize films on to substrate surfaces at low temperatures thereby enabling new combinations of materials such as ceramic coatings on polymer substrates (*Figure 2*). Many methods have been reported for the preparation of conversion coatings [21, 22], polycrystalline thin films [23, 24], epitaxial films [25], mono-molecular layers [26, 27], and superlattices [28].

The unique pressure-temperature interaction of the hydrothermal solution allows the preparation of phases that are difficult to prepare with other synthetic methods. This has been particularly relevant to the manufacturing of single crystals (*Figure 3*). For example, no method other than hydrothermal synthesis can be used to grow large α-quartz single crystals [5]. In general, hydrothermal methods are also used for materials that melt incongruently because such materials cannot be grown with compositional and phase uniformity. Lead zirconate titanate (PZT) is a good example. No compositions with 52/48 Zr/Ti ratios have been reportedly grown from the melt [29].

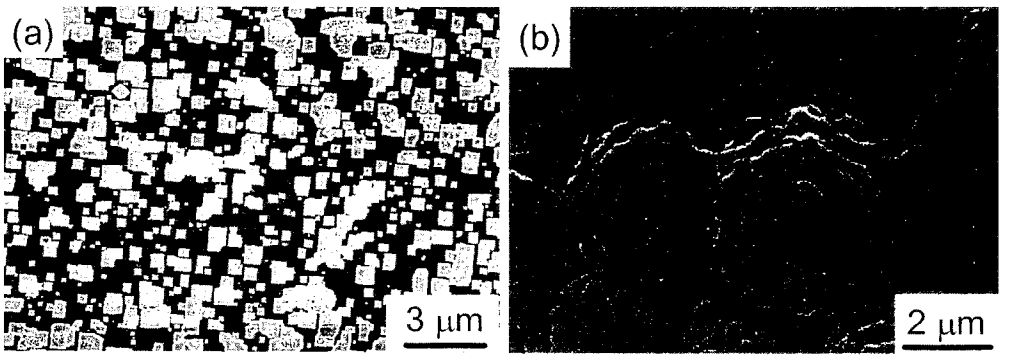

Figure 2. Typical microstructures of $Pb_{1.1}(Zr_{0.7}Ti_{0.3})O_3$ (PZT) epitaxial films deposited on $SrTiO_3$ (100) substrates under hydrothermal conditions at 150°C for 24 h (a) island growth observed at stirring speed of 1200 rpm from a precursor containing 0.33 m Pb-acetate, $ZrOCl_2$, and TiO_2 (total concentration of (Zr+Ti)=0.3 m), and 6 m KOH mineralizer; (b) thin film exhibiting a characteristic spiral growth pattern that was synthesized without stirring, using 0.41 m Pb-acetate, 0.37 m Zr-Ti-hydrous oxide as sources of Pb, Zr, and Ti, respectively, and 10 m KOH mineralizer.

However, such incongruency is not observed when PZT is grown from hydrothermal solution. This has been used to grow thin and thick single crystals on strontium titanate seeds with excellent compositional control [30-32]. Phase fields are often simpler when hydrothermal solutions are used. For instance, in the case of barium titanate, it is the only phase that is stable in hydrothermal solutions while all the other phases with Ba/Ti ratios greater or less than 1:1 are eliminated [33]. The use of mild hydrothermal reaction conditions allows synthesis of metastable compounds which cannot be obtained using classical synthesis methods at high temperatures, as discussed in [34]. Good examples are metastable oxides of tungsten, molybdenum, vanadium, and manganese [14, 34].

Materials synthesized under hydrothermal conditions often exhibit differences in point defects when compared to materials prepared by high temperature synthesis methods. For instance, tungstates of Ca, Ba, and Sr synthesized at room temperature by an hydrothermal-electrochemical method do not contain Schottky defects usually present in similar materials prepared at high temperatures [35], which results in improved luminescent properties. Other types of defects, such as hydroxyl ions substituted for oxygen ions in barium titanate generate barium ion vacancies, which are believed to degrade the dielectric properties [36, 37].

A major advantage of hydrothermal synthesis is the myriad of ways the technology can be hybridized with other processes to gain advantages such as enhancement of reaction kinetics or the ability to make new materials. A great amount of work has been done to enhance hydrothermal synthesis, by hybridizing this method with microwaves, electrochemistry, ultrasound, mechanochemistry, optical radiation, hot-pressing, and many other processes.

Microwave-hydrothermal processing is used mostly for synthesis of ceramic powders. It enhances crystallization kinetics by 1-2 orders of magnitude with respect to standard hydrothermal processing [7]. Additional advantages of this method are very high heating rates and the synthesis of novel phases. The hydrothermal-microwave technique has been used to synthesize different ceramic powders with controlled size and morphology, such as TiO_2, ZrO_2, Fe_2O_3, $BaTiO_3$, hydroxyapatite, etc. [7, 38].

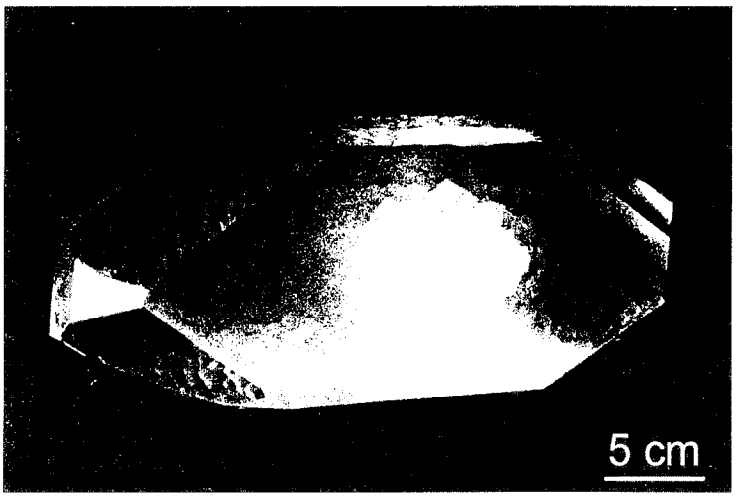

Figure 3. A single crystal of α-quartz, produced commercially using the hydrothermal technique at 350°C under 100 MPa pressure using Na_2CO_3 (aq) as a solvent (photograph provided by J. Radwanski of Sawyer Research Products, Inc).

Hydrothermal-electrochemical synthesis combines the hydrothermal method with electrochemical treatment and involves deposition of polycrystalline oxide films on reactive metal electrode substrates. It is particularly important when crystalline oxide products cannot precipitate from solution in the absence of an applied electrical potential. Highly crystallized ceramic thin films, such as $BaTiO_3$, $SrTiO_3$, $LiNiO_2$, $PbTiO_3$, $CaWO_4$, and $BaMoO_4$ can be deposited on metallic substrates from aqueous solutions at low temperatures 25-200°C within several hours by the hydrothermal-electrochemical method [23, 24]. The hydrothermal-electrochemical technique also enables fabrication of ceramic superlattices. Alternate layers of thallium (III) oxide films (7 nm thick) with different defect structures were deposited using this method. [28]. Monomolecular layers of semiconductors, such as GaAs, CdTe, CdSe, and CdS are made by electrochemical atomic layer epitaxy, which is analogous to molecular beam epitaxy, but instead uses aqueous solutions instead of a vapor phase for transport of growth species [27, 39].

Mechanochemical-hydrothermal synthesis ("wet" mechanochemical) hybridizes hydrothermal synthesis and the classical mechanochemical powder synthesis, which is a solid-state synthesis method that takes advantage of the perturbation of surface-bonded species by pressure to enhance thermodynamic and kinetic reactions between solids [40]. Materials such as $PbTiO_3$ and hydroxyapatite have been made with this approach [40, 41]. It is known that high pressures in excess of 1 GPa catalyze low-temperature solid-state reactions in ceramic materials by orders of magnitude [7]. Mechanochemical-hydrothermal synthesis utilizes the solvency of an aqueous solution, which capitalizes on using the pressure environment provided by the mechanochemical reactor to accelerate one or more the rate-determining steps that limit the lower temperature for hydrothermal reactions such as interfacial reaction, crystal dissolution or dehydroxylation. The mechanochemical activation of slurries can generate localized zones of high temperature (~ 450-700°C) and high pressure due to friction and adiabatic heating of gas bubbles (if present in the slurry), while maintaining the average temperature close to the room temperature [42]. Since any type of mill or comminuting equipment can be used, the mechanochemical-hydrothermal route

offers the potential for process scale-up yet eliminates the need for use of a pressure vessel or external heating. However, control of particle size, morphology and aggregation is a challenge for this method since current methods fail to regulate rates of nucleation, growth and aging, as well as conventional hydrothermal technologies are able to. To address this issue, recent work [43] has incorporated the use of emulsions in mechanochemical-hydrothermal reactors to better regulate nucleation and growth, which resulted in hydroxyapatite that is far less aggregated.

Hydrothermal-sonochemical synthesis hybridizes hydrothermal synthesis with ultrasound (acoustic 20kHz-10MHz). Ultrasound is known to accelerate the reaction kinetics by as much as two orders of magnitude [7]. This has been attributed to to sharp temperature gradients with localized peak temperature zones that are speculated to be as high as 5000 K and localized peak pressure zones of up to 180 MPa, while maintaining the average temperature close to room temperature [44]. These gradients create caviation/bubble collapse events that inhibit the formation of agglomerates or aggregates during crystallization. The sonochemical environment is also considered to alter molecular chemistry (chemical bond scission, generate excited states and accelerate electron transfer steps in chemical reactions), and enhance mass transport and crystallization kinetics. [44]. Hydrothermal-sonochemical synthesis methods have been reported for many ceramic powders ($Ca_{10}(PO_4)_6(OH)_2$, $AlPO_4$, InSb, CdS) and thin films ($Li_2B_4O_7$, $Ba_2TiSi_2O_8$).

Hydrothermal-photochemical synthesis utilizes laser irradiation is to increase growth rates by an order of magnitude for ceramics and 3 orders of magnitude for metals [45, 46]. Moreover, it enables precise patterning of thin films with a resolution of ~1 μm [45, 46], which is essential in the integration of hydrothermal techniques with other device fabrication technologies. Enhancement of the reaction rate can be attributed to temperature, diffusional enhancement due to light-induced thermal-gradients that micro-stir the solution [45, 46], and/or photo-chemistry [47]. Examples of ceramics synthesized by the hydrothermal-photochemical include thin films of Ni-, Zn-, Co-, and Mn-ferrites, Co_3O_4, Tl_2O_3, and Fe_3O_4.

Hydrothermal hot pressing is a simple and effective fabrication technique for shaped ceramics under mild conditions (T=100-350°C, P<25 MPa), within a short reaction time below 1 h, often in only one processing step (reactive hydrothermal sintering or hot pressing). This technique is very useful for solidification of radioactive wastes and sludge ashes [48]. The process involves compacting a ceramic powder or its precursor under hydrothermal conditions either in a special hot-pressing apparatus where uniaxial pressure can be applied or simply in a metal capsule [9, 49]. Another possibility is direct hydrothermal sintering of a pressed pellet of powder. During the hydrothermal treatment, mass transport leading to densification occurs mostly by a dissolution-precipitation mechanism. The resulting materials are usually very porous, but exhibit fairly good mechanical properties. Nevertheless, relative densities as high as 94% have been reported [49]. Low processing temperatures enable the incorporation of organic components that can improve mechanical strength of the porous ceramics. Examples of ceramics synthesized and/or densified by this method include zirconia, titania, silica, calcium carbonate, strontium carbonate, magnesium carbonate, hydroxyapatite, glass, and mica.

1.4. Implementation of hydrothermal synthesis in industry

The advantages of hydrothermal methods provide the means for transforming this emergent technology into a commercially feasible one. For instance, nanopowders used to comprise nanomaterials are primarily synthesized by expensive vapor phase synthesis methods, whose cost drivers are precursors, energy and reactor technology. Development of commercial hydrothermal

processes capable of making similar powders will be a "disruptive" technology that will provide a paradigm shift in the nanomaterials community. The numerous reports in the literature of nanopowder synthesis by hydrothermal methods [17, 50-52] serve as significant evidence that this paradigm shift is inevitable.

Several hydrothermal technologies for ceramic powders have already been developed that demonstrate the commercial potential of this processing route. For the production of single crystals, α-quartz is the best example (*Figure 3*), with a production rate on the order of 3000 tons/year [2] for a wide range of frequency control and optical applications. Potassium titanyl phosphate (KTP) is another single crystal material that is hydrothermally grown for nonlinear optical applications [53, 54]. While this is a great example of a novel advanced material, the annual production rate (estimated as ~1 ton/year [55]) is orders of magnitude lower than for quartz. Perhaps the largest potential growth area for commercialization is ceramic powder production. The widely used Bayer process uses hydrothermal methods to dissolve Bauxite and subsequently precipitate aluminum hydroxide, which is later heat-treated at high temperature to crystallize as α-alumina. In 1989, the worldwide production rate was about 43 million tons/year [56]. The production of perovskite-based dielectrics and zirconia-based structural ceramics is a promising growth area for hydrothermal methods. Corporations such as Cabot Corporation, Sakai Chemical Company, Murata Industries, Ferro Corporation and others have established commercial hydrothermal production processes for making dielectric ceramic powder compositions for capacitors [57]. Unlike the above process for making α-alumina or most ceramic powder manufacturing methods, these hydrothermal powders are crystallized as anhydrous oxides with controlled size and morphology directly from solution.

2. THERMODYNAMIC MODELING-A VIABLE ENGINEERING TOOL FOR HYDROTHERMAL SYNTHESIS

In order for hydrothermal synthesis to become a mainstream technology, engineering approaches must be available to facilitate rapid technology development. A majority of the hydrothermal synthesis work that has been done in the past has used Edisonian trial and error methods for process development. This type of experimental approach suffers from its time-consuming nature and the inability to clearly discern between processes that are controlled by either thermodynamics or kinetics. By designing a hydrothermal process to be thermodynamically favored to form desired products, kinetics limitations of the process can be subsequently resolved. Thermodynamic modeling can be used to design a process to be thermodynamically favored using fundamental principles instead of Edisonian methods. Such models can perform many functions for the design of hydrothermal experiments. First, for a given precursor system, the effects of concentration, temperature and pressure can be explored to define the processing variable space over which the phase(s) of interest are stable. Second, many different types of precursor systems can be compared so that robust and cost-effective processes are designed. Third, experiments can be designed to make materials that have never been previously prepared in hydrothermal solution. Such a design approach requires far fewer experiments than Edisonian methods. Furthermore, with phase space well defined for the material of interest, a range of conditions can be explored for control of reaction and crystallization kinetics for the purpose of developing a process suitable for the desired form of the material (e.g, powder, film, or single crystal). Thus, based on the above arguments, the development of thermodynamic models is the core of a suite of engineering tools useful for accelerating technology development.

In the following sections, the steps involved in the construction of a thermodynamic model, its relevant output, experimental validation, and its use as an engineering tool will be described.

Table I. Reaction equilibria in the Ba-Ti-K-H_2O hydrothermal system with TiO_2, $Ba(OH)_2$ and $Ba(NO_3)_2$ as precursors and KOH as a mineralizer.

$H_2O = H^+ + OH^-$	$BaOH^+ = Ba^{2+} + OH^-$
$H_2O_{(g)} = H_2O$	$Ba(OH)_{2(s)} = Ba^{+2} + 2OH^-$
$BaTiO_{3(s)}+H_2O = Ba^{2+}+ HTiO_3^- + OH^-$	$Ba(OH)_2{\cdot}8H_2O = Ba^{+2} + 2OH^- + 8H_2O$
$Ti^{4+} + H_2O = TiOH^{3+} + H^+$	$Ba(NO_3)_{2(s)} = Ba^{+2} + 2NO_3^-$
$TiOH^{3+} + H_2O = Ti(OH)_2^{2+} + H^+$	$HNO_{3(g)} = HNO_{3(aq)}$
$Ti(OH)_2^{2+} + H_2O = Ti(OH)_3^+ + H^+$	$HNO_{3(aq)} = H^+ + NO_3^-$
$Ti(OH)_3^+ + H_2O = Ti(OH)_{4(aq)} + H^+$	$KOH_{(s)} = K^+ + OH^-$
$Ti(OH)_{4(aq)} + OH^- = HTiO_3^- + 2H_2O$	$KOH{\cdot}H_2O = K^+ + OH^- + H_2O$
$TiO_2(rutile) + 2H_2O = Ti(OH)_{4(aq)}$	$KOH{\cdot}2H_2O = K^+ + OH^- + 2H_2O$
$TiO_2(anatase) + 2H_2O = Ti(OH)_{4(aq)}$	$KNO_{3(s)} = K^+ + NO_3^-$

2.1. Construction of a thermodynamic model

In order to construct a thermodynamic model, we will design a process for barium titanate ($BaTiO_3$) powder synthesis from either barium hydroxide or barium nitrate and titanium oxide with a KOH mineralizer. *Table I* shows all possible chemical reactions, which can take place in the Ba-Ti-K-H_2O hydrothermal system. Nitric acid is added in addition to potassium hydroxide so the formation of ceramic materials in basic and/or acidic environments can also be simulated. For completeness, the data for gaseous species are also included although the gas phase plays a secondary role in this case. *Table I* shows that even a simple hydrothermal system such as Ba-Ti-K-H_2O contains a significant number of species and independent chemical reactions.

Determining the equilibrium concentrations for each of the species requires the use of automated computer-based solution algorithms. These algorithms together with data banks are embedded in the OLI Software [58]. One algorithm serves to obtain equilibrium concentrations of all species in the electrolyte system and another algorithm is used to construct stability and yield diagrams. Stability diagrams concisely represent the thermodynamic state of multicomponent, multiphase aqueous systems over wide ranges of temperature and reagent (precursor) concentrations. In the past, stability diagrams were considered for a limited number of hydrothermal systems by assuming that the aqueous solutions were ideal [59-61]. Such diagrams were of limited utility for synthesis research because the input precursor concentrations and corresponding product yields were not specified. For this reason, Lencka and Riman [62] proposed the use of yield diagrams, which specify the synthesis conditions suitable for quantitative precipitation of the phase of interest. No other solid phases are precipitated within this phase field. At that time, stability and yield diagrams for perovskite-type ceramic materials were constructed manually using point-by-point calculations [62-66]. Software for automating the generation of stability and yield diagrams is now available [58, 67].

Calculations of stability and yield diagrams are based on a thermodynamic model that combines the Helgeson-Kirkham-Flowers-Tanger (HKFT) equation of state for standard-state properties of aqueous species [68, 69] with a non-ideal solution model based on the activity coefficient expressions developed by Bromley [70] and Pitzer [71], and modified by Zemaitis *et al.* [72]. For solid species, standard-state properties are used in conjunction with basic thermodynamic relationships. Fugacities of components in the gas phase are calculated from the Redlich-Kwong-Soave equation of state [73]. Details of this thermodynamic model were previously given with an emphasis on the hydrothermal synthesis of ceramic materials [62, 63, 72, 74, 75].

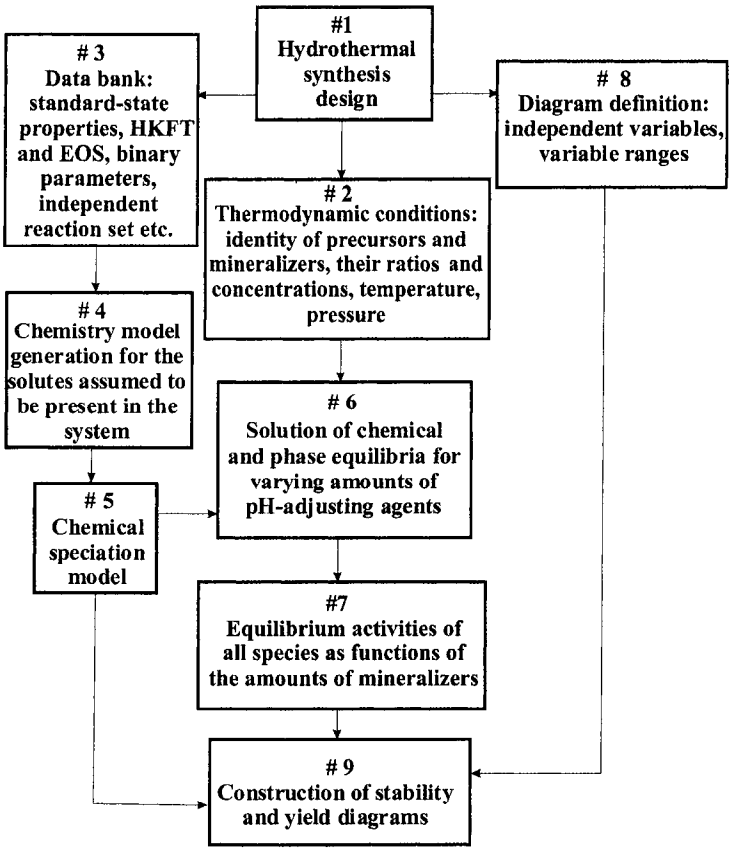

Figure 4. Flow chart for OLI software used for generating stability and yield diagrams.

2.2. Methodology for generating stability and yield diagrams

Figure 4 shows an overall scheme of the program for generating stability and yield diagrams. First, the desired product and components of the hydrothermal system have to be defined (#1). Thus, the identities of the precursors, mineralizers and other additives needed for the synthesis of a required solid phase need to be specified. This information is used as input data, along with the range of reagent concentrations, temperature and pressure specified by the user (#2). It is important that there is a data bank that is relevant for all the components in the system. The software has a comprehensive data bank (#3), which contains standard-state thermochemical properties and independent reaction sets for all species, Helgeson-Kirkham-Flowers-Tanger equation of state parameters for aqueous species, and Redlich-Kwong-Soave equation of state parameters for gaseous species. The software also stores binary parameters for ion-ion, ion-neutral and neutral-neutral species interactions. Standard-state properties used in the data bank were described previously [63, 75]. It should be noted, however, that the standard-state properties and parameters are frequently obtained by regressing numerous kinds of thermodynamic data. These data include vapor pressures, osmotic coefficients, activity coefficients, enthalpies and heat capacities of solutions, and solubilities and heat capacities of solids. When data is not available in the OLI data bank for the specified hydrothermal system, a private data bank must be constructed. The literature can be

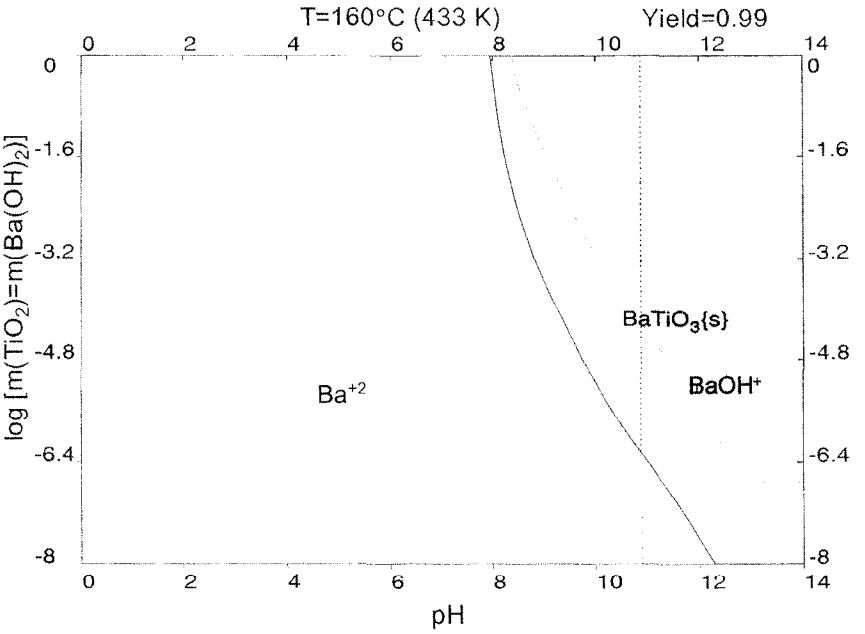

Figure 5. Calculated yield diagram for the Ba-Ti-K-H_2O system at 433 K as a function of the equilibrium solution pH. $Ba(OH)_2$ and TiO_2 (rutile) are used as precursors and the ratio of Ba/Ti is equal to 1. The solid line denotes the incipient precipitation boundary for $BaTiO_3$; in the area above the solid line, $BaTiO_3$ and TiO_2 coexist. The shaded area corresponds to the $BaTiO_3$ yield >99%. The dotted line separates regions dominated by different aqueous species, which in this case are Ba^{2+} and $BaOH^+$.

consulted for data, as well as several methods for estimating thermochemical data [76, 77]. The chemistry model generation step (#4) creates the species and reactions that are possible with the given components of the system. All possible combinations of ions, neutral complexes and solids are considered in this step. The chemical speciation model (#5) is a set of equations, which contains chemical equilibrium equations, phase equilibrium equations, mass balance and electroneutrality equations. Once the thermodynamic conditions are specified (#2), the chemical speciation model is solved (#6). Equilibrium concentrations of all species are calculated as a function of processing variables (e.g. mineralizer concentration) (#7). This gives the equilibrium composition of a specific set of reaction conditions, but in order to understand the overall behavior of the system, computations must be performed over a wide range of conditions. For this purpose, we specify the processing variables of interest (#8). The OLI software offers a flexible choice of independent variables as x- and y-axes of stability and yield diagrams, which include precursor and mineralizer concentrations, solution pH and temperature, in addition to the electrochemical potential, the latter being used for the simulation of corrosion. In the case of yield diagrams, the yield value (e.g., 99, 99.9 and 99.95 %) of the desired material must be chosen. Stability and yield diagrams can then be generated (#9).

2.3. Examples of stability and yield diagrams

Figure 5 presents yield diagram calculated at 433 K for the hydrothermal system obtained by mixing barium hydroxide and titanium dioxide with a stoichiometric molar Ba/Ti ratio equal to

one. The total input concentration of the Ba precursor and the solution pH adjusted by KOH are used as independent variables. The input concentration of the metal precursor takes into account all Ba-containing solution and solid species because we are concerned not only with the equilibrium concentration of species in saturated solution, but also with the conversion of the precursor system into a phase-pure product. It should be noted that all concentrations are expressed in molality (i.e. number of mols per 1 kg of H_2O) because it can be measured more accurately and precisely than molarity. The solid curve in *Figure 5* corresponds to the incipient precipitation (solubility curve) boundary for $BaTiO_3$. In our calculations, an equilibrium point is assumed to lie on the incipient precipitation boundary when less than 0.25% of the precursor is reacted to form a solid phase. Only one point on the solubility curve of $BaTiO_3$ corresponds to the solubility of barium titanate in water and this solubility is equal to about $8.6 \cdot 10^{-4}$ m at 433 K, which corresponds to a pH of 8.7. The pH values correspond to the temperature of the experiment. For example, pH values in alkaline solutions at 433-473 K are 2-3 pH units lower than those for the same solutions at room temperature. The formation of $BaTiO_3$ is dependent on pH. Crystalline $BaTiO_3$ can be obtained at pH higher than ca. 8.0 for the input concentration of TiO_2 equal to 1 m. The stability of $BaTiO_3$ also increases with rising pH, which means, the solubility of barium titanate decreases with increasing pH. At the solubility curve, the yield of barium titanate is very small and it increases as we move beyond the solubility curve into the solid-liquid region, which reaches at least 99% in the shaded area of *Figure 5*. The yield is calculated by dividing the number of moles of the product by the total number of moles of the input metal precursor. The shaded area in *Figure 5* shows the range of input precursor concentrations and equilibrium pH that can produce 99%+ phase-pure $BaTiO_3$ at 433 K.

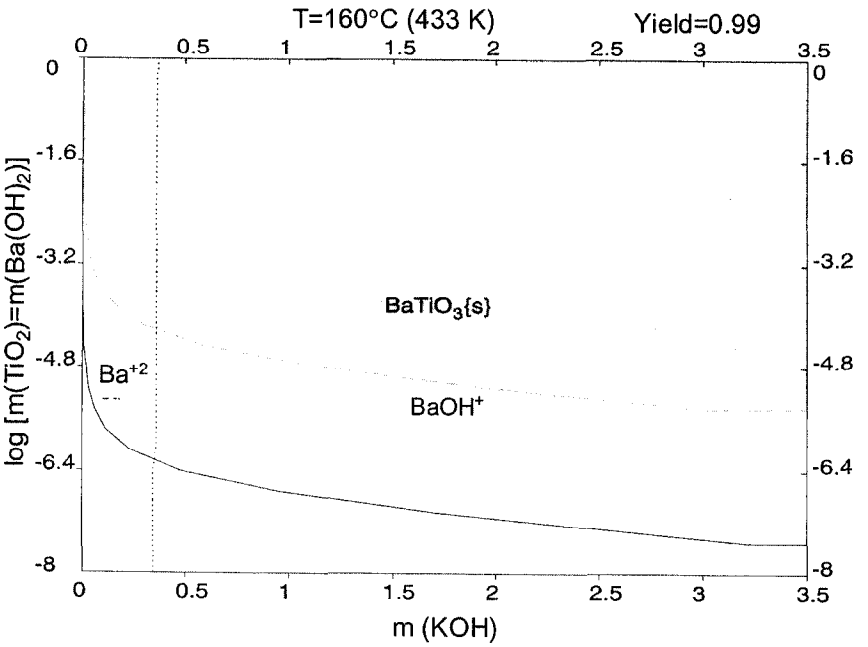

Figure 6. Calculated yield diagram for the Ba-Ti-K-H_2O system at 433 K as a function of the input molality of KOH. $Ba(OH)_2$ and TiO_2 (rutile) are used as precursors and the ratio of Ba/Ti is equal to 1. The solid line denotes the incipient precipitation boundary for $BaTiO_3$; in the area above the solid line, $BaTiO_3$ and TiO_2 coexist. The shaded area corresponds to the $BaTiO_3$ yield >99%. The dotted line separates regions dominated by different aqueous species, which in this case are Ba^{2+} and $BaOH^+$.

The dotted line on the yield diagram corresponds to the loci where two aqueous species have equal concentrations, which in this case corresponds to Ba^{2+} and $BaOH^{+}$. At 433 K, Ba^{2+} dominates at pH below 10.8 and it becomes hydrolyzed to $BaOH^{+}$ above this pH. There are also titanium complexes present in this system (cf., *Table I*). However, their concentrations within the stability region corresponding to 99% yield of barium titanate are very small (~10^{-9}-10^{-8} m) and do not change significantly with mineralizer concentration or increases in temperature. Thus, this data is not shown in *Figure 5* for clarity. As pH increases (increasing mineralizer concentrations), even the amount of soluble barium decreases to very low values.

The optimum conditions for the precipitation of barium titanate are also shown in *Figure 6*, which is a plot that shows input concentrations on both x and y axes. The total input concentrations of Ba and Ti precursors at a fixed molar ratio (Ba/Ti=1) are shown on the y-axis and pH is replaced with the molality of a mineralizer (KOH) as the x-axis variable. In contrast to the diagrams with equilibrium pH as an independent variable, these diagrams are more practical because they directly specify the molalities of precursors and mineralizer that are needed to obtain a specified yield of product. The solid line in *Figure 6* denotes the incipient precipitation boundary for barium titanate. In the area above the solid line, barium titanate and titanium oxide coexist. As we move closer to the shaded area, the yield of barium titanate increases while the amount of titanium dioxide decreases. The shaded region shows the optimum synthesis conditions (i.e., input molality of barium hydroxide, titanium dioxide and potassium hydroxide) for the formation of phase-pure barium titanate (yield greater than 99%) at 433 K. The amount of KOH necessary to form phase-

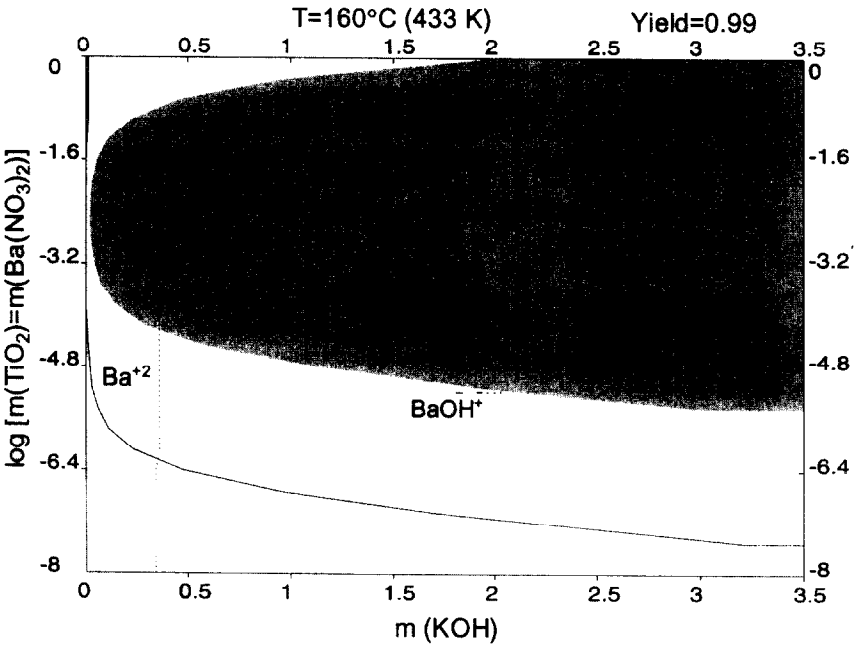

Figure 7. Calculated yield diagram for the Ba-Ti-K-H_2O system at 433 K as a function of the input molality of KOH. $Ba(NO_3)_2$ and TiO_2 (rutile) are used as precursors and the ratio of Ba/Ti is equal to 1. The solid line denotes the incipient precipitation boundary for $BaTiO_3$; in the area above the solid line, $BaTiO_3$ and TiO_2 coexist. The shaded area corresponds to the $BaTiO_3$ yield >99%. The dotted line separates regions dominated by different aqueous species, which in this case are Ba^{2+} and $BaOH^{+}$.

pure $BaTiO_3$ from $Ba(OH)_2$ increases with a decrease of input molalities of precursors. For the input concentration of $Ba(OH)_2$ above 0.09 m, no mineralizer is necessary to obtain phase-pure $BaTiO_3$. This is because the necessary concentration of OH^- groups is provided by the barium hydroxide precursor to drive the reaction for barium titanate formation to completion.

When barium nitrate and titanium dioxide with a molar ratio Ba/Ti equal to 1.0 are used as precursors and KOH is used to adjust pH, a qualitatively similar diagram is obtained (see *Figure 7*). The position of the incipient precipitation line does not depend on the precursor identity and therefore, remains the same, however, the area of the 99% yield of barium titanate has a different shape. At low concentrations of barium nitrate (below 0.004 m), the same amount of KOH is necessary to obtain more than 99% of $BaTiO_3$, as in the case of barium hydroxide. At concentrations of precursors above about 0.004 m, the amount of the mineralizer increases proportionally to the amount of precursors. This is because in concentrated solutions, two moles of OH^- are consumed for the synthesis of one mole of $BaTiO_3$ and only a relatively small amount of additional OH^- is necessary to ensure a pH sufficient for $BaTiO_3$ stability. *Figure 7* shows that a mineralizer will always be necessary for the hydrothermal synthesis of $BaTiO_3$ if barium nitrate is used as the precursor. If precursors with the Ba/Ti ratio above 1 are used, the area of phase-pure $BaTiO_3$ 99% yield region widens and moves towards the incipient precipitation line. In general, it is possible to vary the relative amounts of precursors in order to decrease or eliminate the necessary amount of mineralizer for the precipitation of a pure material [67, 75].

2.4. Thermodynamic model validation and utility

Thermodynamic modeling has benefited the materials community by being enabling the preparation of new materials, streamlined experimental design, process optimization for making phase-pure materials and designated processing variable space for particle size and morphology control. To demonstrate this utility, we will discuss our research focusing on the synthesis of perovskite materials useful for dielectric and piezoelectric applications [62, 63, 76]. The research always starts with the computation of stability and yield equilibrium diagrams. After the diagrams are generated, experiments are chosen to test the phase boundaries that are relevant to the material of interest. For instance, diagrams were generated for $Na_{0.5}Bi_{0.5}TiO_3$ (NBT) and $K_{0.5}Bi_{0.5}TiO_3$ (KBT), which prior to our research have never be previously prepared via hydrothermal methods. The diagrams calculated at 200°C postulated that NBT was stable at pH>11 (*Figure 8*) and KBT was stable at pH>12 for wide ranges of titanium and bismuth precursor concentrations. These conditions correspond to the NaOH concentrations greater than 4 m for NBT and KOH concentrations above 6 m for KBT (*Figure 9*), where yields higher than 99% are expected. The data points on these *Figures 8* and *9* show experimental data that demonstrates that the recommended reaction conditions and experimentally obtained phase assemblages are entirely consistent with the expected phase assemblages based on thermodynamic calculations [78].

The above discussion shows how thermodynamics can be used to quickly identify systems that are suitable for hydrothermal methods. However, calculations can also be used to quickly identify materials that cannot be prepared with hydrothermal methods due to thermodynamic instability. Two good examples are lead magnesium niobate (PMN) and lead zinc niobate (PZN). Diagrams computed at temperatures of 200°C for hydrothermal systems targeted for PMN or PZN failed to show any perovskite phase field (*Figures 10* and *11*). The experiments were performed to test these thermodynamic models, and the phase fields predicted by thermodynamic calculations were confirmed, which indicated that these phases cannot be prepared with hydrothermal methods under mild reaction conditions.

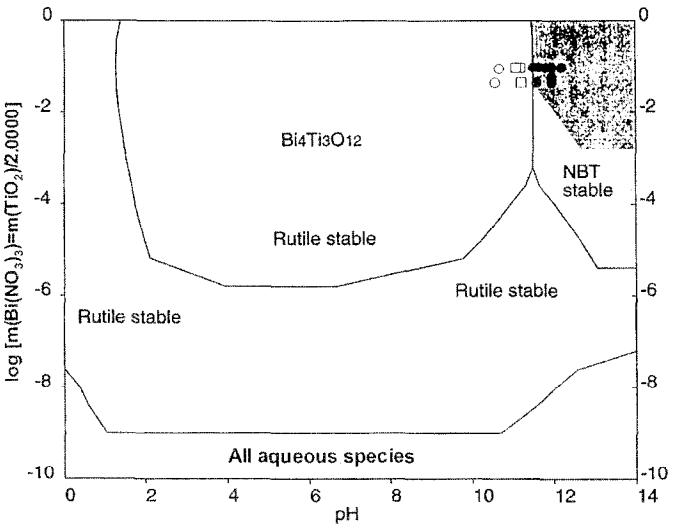

Figure 8. Calculated yield diagram for the Na-Bi-Ti-H_2O system at 200°C as a function of solution pH. The symbols denote experimentally obtained phase assemblages corresponding to the reaction conditions specified by the equilibrium diagram: ○, $Bi_4Ti_3O_{12}$+TiO_2; □, $Bi_4Ti_3O_{12}$+TiO_2+$Na_{0.5}Bi_{0.5}TiO_3$; ●, $Na_{0.5}Bi_{0.5}TiO_3$. The shaded area corresponds to the $Na_{0.5}Bi_{0.5}TiO_3$ yield >99%.

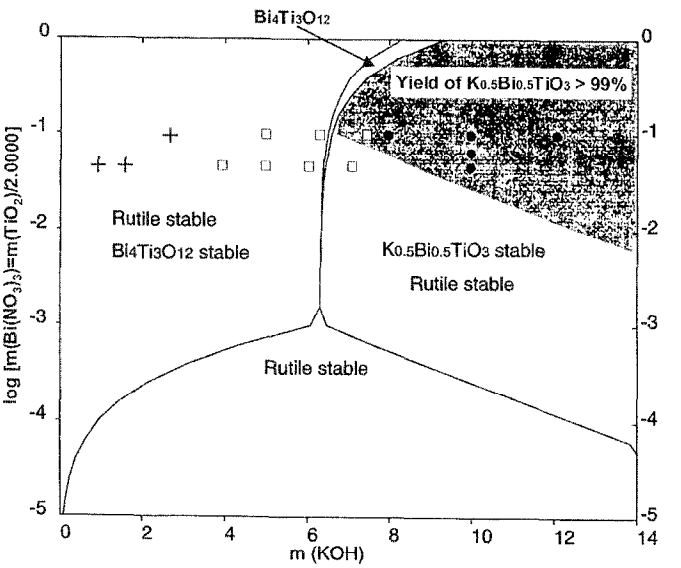

Figure 9. Calculated yield diagram for the K-Bi-Ti-H_2O system at 200°C as a function of KOH concentration. The symbols denote experimentally obtained phase assemblages corresponding to the reaction conditions specified by the equilibrium diagram: +, $Bi_4Ti_3O_{12}$+TiO_2+an unknown phase; □, $Bi_4Ti_3O_{12}$+TiO_2+$K_{0.5}Bi_{0.5}TiO_3$; ●, $K_{0.5}Bi_{0.5}TiO_3$. The shaded area corresponds to the $K_{0.5}Bi_{0.5}TiO_3$ yield >99%.

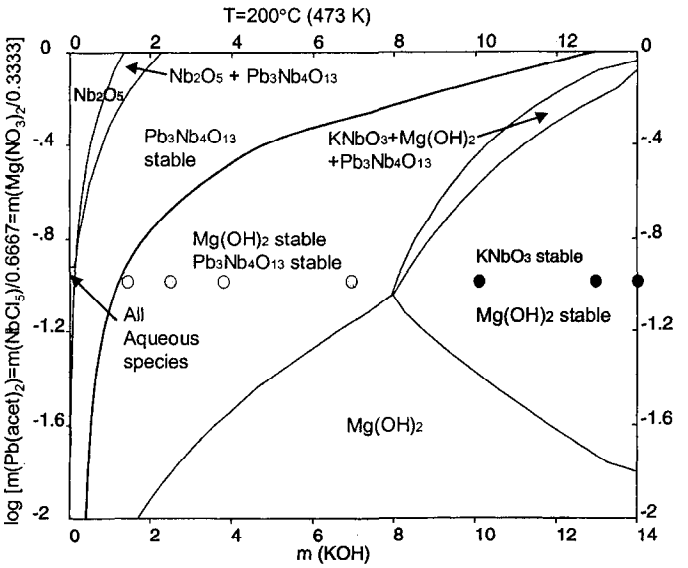

Figure 10. Computed stability diagram for the Pb-Mg-Nb-K-H_2O system at 200°C where input precursor concentration is plotted as a function of mineralizer (KOH) concentration. The symbols denote experimentally obtained phase assemblages corresponding to the reaction conditions specified by the equilibrium diagram: ○, $Mg(OH)_2$+$Pb_3Nb_4O_{13}$; ●, $KNbO_3$+$Mg(OH)_2$.

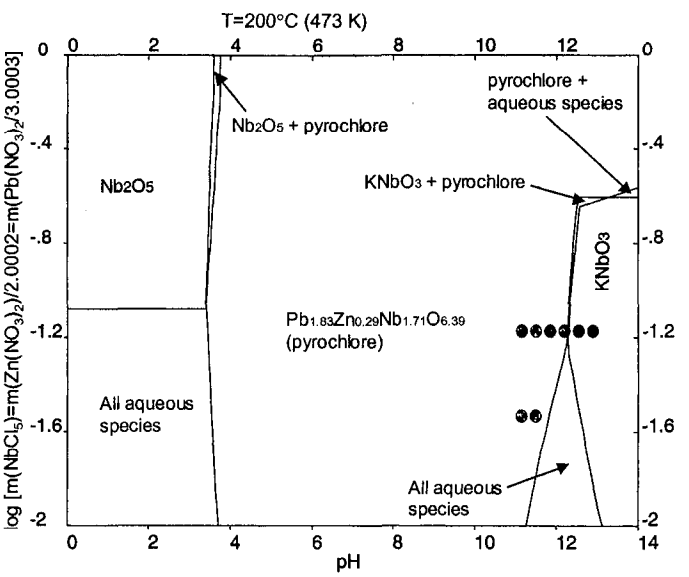

Figure 11. Computed stability diagram for the Pb-Zn-Nb-K-H_2O system at 200°C where input precursor concentration is plotted as a function of equilibrium pH. The symbols denote experimentally obtained phase assemblages corresponding to the reaction conditions specified by the equilibrium diagram: ○,$Pb_{1.83}Zn_{0.29}Nb_{1.71}O_{6.39}$ (pyrochlore); ●, $KNbO_3$.

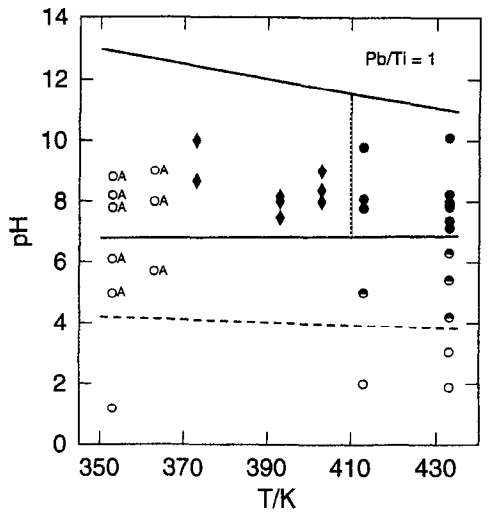

Figure 12. Solid products of hydrothermal reactions of Pb-acetate and/or $Pb(NO_3)_2$ and TiO_2 for Pb/Ti=1 at different temperatures and pH values: ●, crystalline $PbTiO_3$; A, amorphous $PbTiO_3$; ○, TiO_2; ●/○, $PbTiO_3$+TiO_2; ◆, $PbTiO_3$+TiO_2+PbO+ $Pb_2Ti_2O_6$. The horizontal dashed line denotes the beginning of precipitation of $PbTiO_3$ and the horizontal solid lines encompass the region where the calculated yield of $PbTiO_3$ exceeds 99.99%. This region is divided by a vertical dotted line, which is a threshold temperature above which the process is thermodynamically controlled and below which the process is controlled by sluggish kinetics.

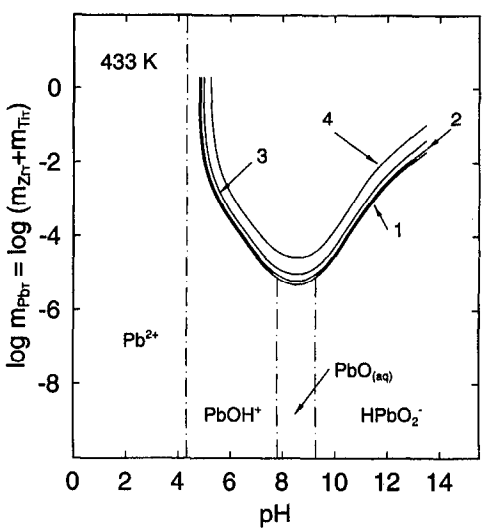

Figure 13. Calculated stability diagrams for the system Pb-Zr-Ti-H_2O at 150°C. The incipient precipitation lines are shown for (1) $PbZr_{0.46}Ti_{0.54}O_3$, (2) $PbZr_{0.52}Ti_{0.48}O_3$, (3) $PbZr_{0.60}Ti_{0.40}O_3$, and (4) $PbZr_{0.75}Ti_{0.25}O_3$. Pb-acetate, TiO_2, and ZrO_2 are used as starting materials and the ratio of total molalities Pb/(Zr+Ti)=1.0. The dashed dotted lines separate regions dominated by different aqueous species.

Computed phase diagrams can also be used to determine the temperature where kinetically-controlled processes transition to thermodynamically-controlled ones. *Figure 12* shows thermodynamically stable phases with temperature as the independent variable and pH as the dependent variable for the Pb-Ti-H_2O system. The vertical line at ~137°C shows the transition temperature below which thermodynamics cannot predict the phase assemblage (the phases are often amorphous or consisting of mixtures of reactants and intermediates). Above this temperature, thermodynamics is very effective in predicting the phase assemblage.

The interdependence between product composition and the requisite reaction conditions can be studied with thermodynamic calculations. A good example is $Pb(Zr_xTi_{1-x})O_3$ (PZT) with its broad range of solid solutions. Stability fields are shown in *Figure 13* for both solid phases and dominant species with pH as the dependent variable and precursor concentration as the dependent variable. Incipient precipitation boundaries are shown for several x values that correspond to 0.46, 0.52 and 0.75, which were chosen since they correspond to tetragonal, morphotropic phase boundary (mixture of tetragonal and rhombohedral) and rhombohedral compositions, respectively. These calculations reveal that changing the relative fraction of zirconium and titanium in PZT does not change the hydrothermal conditions required for thermodynamic stability to a very significant degree. Thus, computations for one specific PZT composition are probably relevant for a wide range of compositions. Our work has validated that since we have found the conditions to be comparable for both morphotropic and rhombohedral compositions.

Validated equilibrium diagrams can be used to define the range of processing variable space (reaction conditions) to control particle size and size distribution for a given phase. For example, changing the concentration of tetramethylammonium hydroxide (TMAH) from 0.5 to 1.0 m can change the PZT powder morphology from a fiber-like morphology to a cube-shaped morphology (*Figure 1)* [79]. Similarly, nanosized hydroxyapatite powders with a range of sizes and aspect ratios can be prepared by applying different additives to the crystallization environment (*Figure 1*).

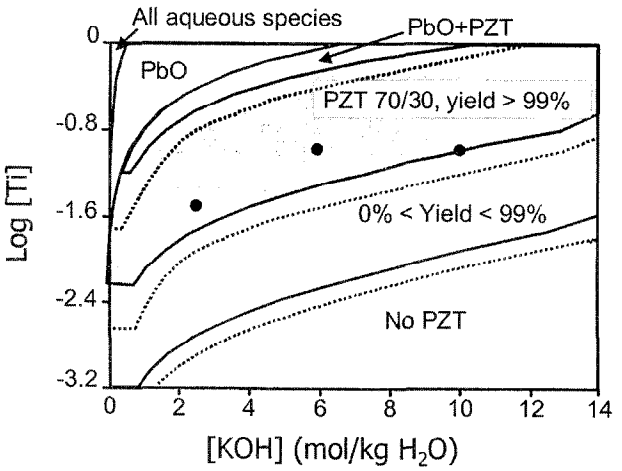

Figure 14. Phase equilibria in the Pb-Zr-Ti-K-H_2O system at 150°C (solid lines) and at 300°C (dotted lines) as functions of precursor and mineralizer concentrations. Pb/(Zr+Ti)=1.1 has been assumed in the calculations. The shaded region corresponds to a $Pb(Zr_{0.7}Ti_{0.3})O_3$ yield of more than 99% at 150°C. The symbol, ●, denotes experimental reaction conditions where phase-pure $Pb(Zr_{0.7}Ti_{0.3})O_3$ was formed.

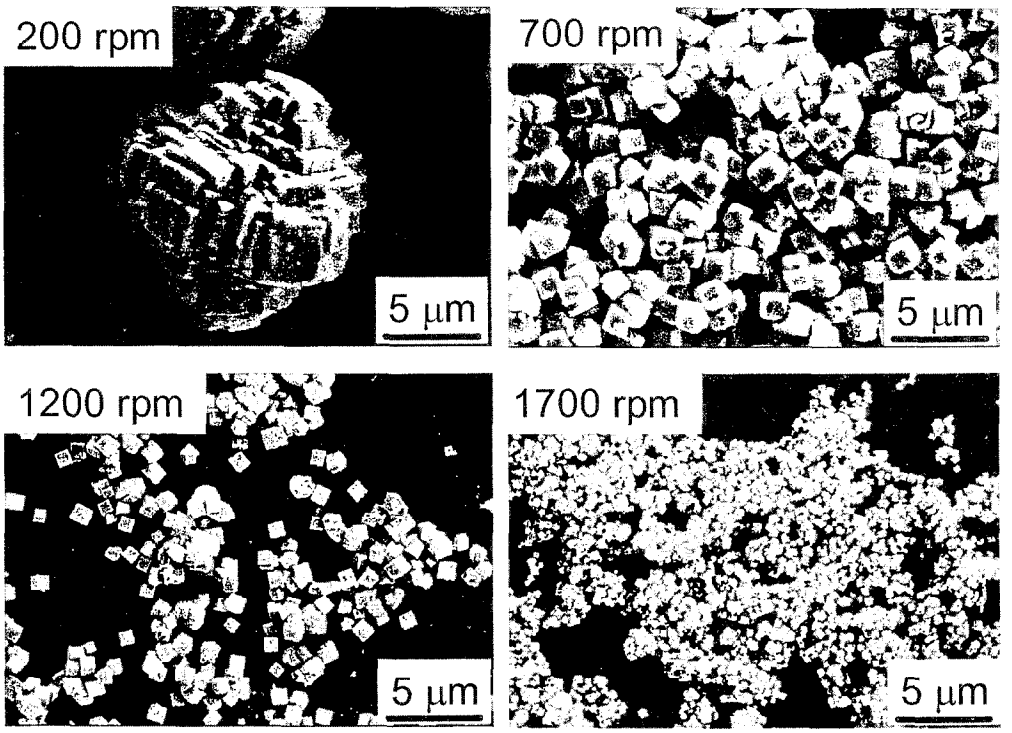

Figure 15. PZT crystals synthesized hydrothermally at 150°C for 24 h. In all cases lead acetate, crystalline TiO_2, and $ZrOCl_2$ were used as sources of Pb, Ti, and Zr, respectively. Total concentration of (Zr+Ti) was 0.3 m, concentration of the KOH mineralizer was 6 m, and the Pb:Zr:Ti ratio was 1.1:0.70:0.30. Stirring speeds were as marked.

Processing variables such as temperature, pH, reactant concentration are thermodynamic variables but also influence both reaction and crystallization kinetics. However, it should be realized that non-thermodynamic variables associated with the reactors used to crystallize the ceramic powders are also important when operating in thermodynamically-controlled processing variable space. Using *Figure 14* to define the phase space, increasing the stirring speed from 200 to 1700 rpm can change the particle size of PZT crystals from over 10 microns to a nanosized range (*Figure 15*) [32]. This is a very important capability of hydrothermal synthesis, since it allows dialing in a specific particle size or morphology for a process and changing it to suit the requirements of the user. Furthermore, it simplifies the process greatly since all other reaction conditions are held constant.

3. REFERENCES

[1] K. F. E. Schafthaul, Gelehrte Anzeigen Bayer. Akad., 20 (1845) 557-593.
[2] K. Byrappa, M. Yoshimura, Handbook of Hydrothermal Technology, Noyes Publications/William Andrew Publishing LLC, Norwich, NY, U.S.A. (2001).
[3] M. J. G. Van Hout, J. C. Verplanke, J. M. Robertson, Mater. Res. Bull., 10 (1975) 125-132.
[4] M. Yoshimura, W. L. Suchanek, K. Byrappa, MRS Bull., 25 (2000) 17-25.

[5] R. A. Laudise, Chem. & Eng. News, September 28 (1987) 30-43.
[6] E. D. Kolb, R. L. Barns, R. A. Laudise, J. Crystal Growth, 50 (1980) 404-418.
[7] R. Roy, J. Solid State Chem., 111 (1994) 11-17.
[8] G. Demazeau, In Proceedings of Joint ISHR & ICSTR, Kochi, Japan, July 25-28, 2000 (ed K. Yanagisawa and Q. Feng), Nishimura Tosha-do Ltd., Kochi, Japan, (2002) pp. 1-5.
[9] S. Sômiya, ed. Hydrothermal Reactions for Materials Science and Engineering. An Overview of Research in Japan. Elsevier Science Publishers Ltd., London (1989).
[10] J. O. Eckert Jr., C. C. Hung-Houston, B. L. Gersten, M. M. Lencka, R. E. Riman, J. Am. Ceram. Soc., 79 (1996) 2929-2939.
[11] M. M. Lencka, R. E. Riman, Chem. Mater., 7 (1995) 18-25.
[12] W. Suchanek, H. Suda, M. Yashima, M. Kakihana, M. Yoshimura, J. Mater. Res., 10 (1995) 521-529.
[13] T. Bein, In Supramolecular Architecture. Synthetic Control in Thin Films and Solids, ACS Symp. Series. Vol. 499 (ed T. Bein) (1992) pp. 274-293.
[14] M. S. Whittingham, Curr. Opinion Solid State & Mater. Sci., 1 (1996) 227-232.
[15] A. Szymanski, E. Abgarowicz, A. Bakon, A. Niedbalska, R. Salacinski, J. Sentek, Diamond and Related Materials, 4 (1995) 234-235.
[16] W. L. Suchanek, J. Libera, Y. Gogotsi, M. Yoshimura, J. Solid State Chem., 160 (2001) 184-188.
[17] T. Sugimoto, Fine Particles, Synthesis, Characterization, and Mechanisms of Growth, Marcel-Dekker, Inc., New York, 2000.
[18] R. E. Riman, High Performance Ceramics: Surface Chemistry in Processing Technology, edited by R. Pugh and L. Bergström, Marcel-Dekker, NY, (1993) pp. 29-69.
[19] T. A. Ring, Fundamentals of Ceramic Powder Processing and Synthesis, Academic Press, San Diego, CA (1996).
[20] K. Haberko, W. Pyda, In Science and Technology of Zirconia II, Advances in Ceramics Vol. 12 (ed N. Claussen, M. Ruhle, A. H. Heuer), (1984) pp. 774-783.
[21] R. E. Riman, S-B. Cho, U.S. Patent 6,159,552, December 12, 2000.
[22] R. E. Riman, S-B. Cho, U.S. Patent 6,322,898, November 27, 2001.
[23] W. Suchanek, M. Yoshimura, J. Am. Ceram. Soc., 81 (1998) 2864-2868.
[24] M. Yoshimura, W. Suchanek, Solid State Ionics, 98 (1997) 197-208.
[25] F. F. Lange, Science, 273 (1996) 903-909.
[26] J. H. Fendler, F. C. Meldrum, Adv. Mater., 7 (1995) 607-632.
[27] I. Villegas, J. L. Stickney, J. Electrochem. Soc., 139 (1992) 686-694.
[28] J. A. Switzer, C. J. Hung, B. E. Breyfogle, M. G. Shumsky, R. Vanleeuwen, T. D. Golden, Science, 264 (1994) 1573-1576.
[29] R. Clarke, R. W. Whatmore, J. Crystal Growth, 33 (1976) 29-38.
[30] P. Pinceloup, K. M. Mikulka, R. E. Riman, P. E. Burgener, L. E. McCandlish, M. Lencka, Perovskite Oxides for Electronics, Energy Conversion and Energy Efficient Applications, Ceramic Transactions, Volume 104, edited by W. Wong-Ng, T. Holesinger, G. Riley, T. Guo, American Ceramic Society, Westerville, OH (2000) pp. 253-260.
[31] M. Oledzka, M. Lencka, P. Pinceloup, K. Mikulka-Bolen, L. E. McCandlish, R. E. Riman, Chemistry of Materials, in press, August 2002.
[32] W. L. Suchanek, M. Oledzka, K. Mikulka-Bolen, R. L. Pfeffer, M. Lencka, L. McCandlish, R. E. Riman, (2002). In Proceedings of Fifth International Conference on Solvothermal Reactions (ICSTR), East Brunswick, New Jersey, July 22-26, 2002 (ed. R. E. Riman), pp. 159-164.
[33] Y. Suwa, Y. Sugimoto, S. Naka, Funtai Oyobi Fummatsu-Yakin, 25 (1978) 20-23.
[34] M. Figlarz, Perspect. Solid State Chem., (1995) 1-21.

[35] W. S. Cho, M. Yashima, M. Kakihana, A. Kudo, T. Sakata, M. Yoshimura, Appl. Phys. Lett., 66 (1995) 1027-1029.
[36] Y. Sakabe, N. Wada, Y. J. Hamaji, Korean Phys. Soc., 32 (1998) S260-S264.
[37] D. Hennings, S. J. Schreinmacher, European Ceram. Soc., 9 (1992) 41-46.
[38] S. Komarneni, R. Roy, Q. H. Li, Mater. Res. Bull., 27 (1992) 1393-1405.
[39] L. P. Colletti, B. H. Flowers Jr., J. L. Stickney, J. Electrochem. Soc., 145 (1998) 1442-1449.
[40] W. L. Suchanek, P. Shuk, K. Byrappa, R. E. Riman, K. S. TenHuisen, V. F. Janas, Biomaterials, 23 (2002) 699-710.
[41] K. Hamada, M. Senna, J. Mater. Sci., 31 (1996) 1725-1728.
[42] N. V. Kosova, A. Kh. Khabibullin, V. V. Boldyrev, Solid State Ionics, 101-103 (1997) 53-58.
[43] C.-W. Chen, R. E. Riman, submitted to Chem. Mater (2002).
[44] D. Peters, J. Mater. Chem., 10 (1996) 1605-1618.
[45] J. C. Puippe, R. E. Acosta, R. J. von Gutfeld, J. Electrochem. Soc., 128 (1981) 2539-2545.
[46] T. Itoh, S. Hori, M. Abe, Y. Tamaura, J. Appl. Phys., 69 (1991) 5911-5914.
[47] Y. Matsumoto, M. Fujisue, T. Sasaki, J. Hombo, M. Nagata, J. Electroanalyt. Chem., 369 (1994) 251-254.
[48] K. Yanagisawa, M. Nishioka, N. Yamasaki, Am. Ceram. Soc. Bull., 64 (1985) 1563-1567.
[49] N. Yamasaki, T. Weiping, K. Yanagisawa, J. Mater. Res., 8 (1993) 1972-1976.
[50] M. Yoshimura, S. Sômiya, Materials Chemistry and Physics, 61 (1999) 1-8.
[51] H. Xu, L. Gao, J. Guo, J. European Ceram. Soc., 22 (2002) 1163-1170.
[52] L. Yan, Y. Li, Z-X. Deng, J. Zhuang, X. Sun, Int. J. Inorg. Mater., 3 (2001) 633-637.
[53] F. Ahmed, R. F. Belt, G. Gashurov, J. Appl. Phys., 60 (1986) 839-841.
[54] F. C. Zumsteg, J. D. Bierlein, T. E. Gier, J. Appl. Phys., 47 (1976) 4980-4985.
[55] R. Uhrin, (2002). Private communication.
[56] A. J. Brown, J. Bultitude, J. M. Lawson, H. D. Winbow, S. Witek, Engineered Materials Handbook, vol 4, Ceramics and Glasses, ASM International, U.S.A. (1991) pp. 43-51.
[57] W. J. Dawson, Ceram. Bull., 67 (1988) 1673-1678.
[58] OLI Systems, Inc. Software (1996-2002).
[59] Ch. F. Baes Jr., R. E. Mesmer, The Hydrolysis of Cations, Wiley-Interscience, New York, NY, U.S.A. (1976).
[60] J. H. Adair, R. P. Denkiewicz, F. J. Arriagada, K. Osseo-Asare, in Ceramic Transactions, vol. I, Ceramic Powder Science IIA, American Ceramic Society; (ed. G. L. Messing, E. R. Fuller Jr., H. Hausner) Westerville, OH, (1988) pp. 135-145.
[61] K. Osseo-Asare, F. J. Arriagada, J. H. Adair, in Ceramic Transactions, vol. I, Ceramic Powder Science IIA, American Ceramic Society; (ed. G. L. Messing, E. R. Fuller, Jr., H. Hausner); Westerville, OH, (1988) pp. 47-53.
[62] M. M. Lencka, R. E. Riman, J. Am. Ceram. Soc., 76 (1993) 2649-2659.
[63] M. M. Lencka, R. E. Riman, Chem. Mater., 5 (1993) 61-70.
[64] M. M. Lencka, R. E. Riman, Ferroelectrics, 151 (1994) 159-164.
[65] M. M. Lencka, R. E. Riman, Chem. Mater., 7 (1995) 18-25.
[66] M. M. Lencka, A. Anderko, R. E. Riman, J. Am. Chem. Soc., 78 (1995) 2609-2618.
[67] M. M. Lencka, E. Nielsen, A. Anderko, R. E. Riman, Chem. Mater., 9 (1997) 1116-1125.
[68] H. C. Helgeson, D. H. Kirkham, G. C. Flowers, Am. J. Sci., 281 (1981) 1249-1428.
[69] J. C. Tanger, H. C. Helgeson, Am. J. Sci., 288 (1988) 19-98.
[70] L. A. Bromley, AIChE J., 19 (1973) 313-20.
[71] K. S. Pitzer, J. Phys. Chem., 77 (1973) 268-277.
[72] J. F. Zemaitis Jr., D. M. Clark, M. Rafal, N. C. Scrivner, Handbook of Aqueous Electrolyte Thermodynamics: Theory & Application, AIChE, New York, NY (1986).
[73] G. Soave, Chem. Eng. Sci., 27 (1972) 1197-1203.

[74] M. Rafal, J. W. Berthold, N. C. Scrivner, S. L. Grise, in Models for Thermodynamic and Phase Equilibria Calculations, M. Dekker, New York, NY, U.S.A, (1995) pp. 601-670.
[75] M. M. Lencka, R. E. Riman, in Encyclopedia of Smart Materials, Chapter X, Wiley&Sons, New York, (2002) in press.
[76] M. M. Lencka, R. E. Riman, Thermochimica Acta, 256 (1995) 193-203.
[77] J. O. Eckert, Jr., I.-C. Lin, M. M. Lencka, P. M. Bridenbaugh, A. Navrotsky, R. A. Laudise, R. E. Riman, Thermochimica Acta, 286 (1996) 233-243.
[78] M. M. Lencka, M. Oledzka, R. E. Riman, Chem. Mater., 12 (2000) 1323-1330.
[79] S.-B. Cho, M. Oledzka, R. E. Riman, J. Crystal Growth, 226 (2001) 313-326.

(Article reçu le 13/08/02, sous forme définitive le 18/10/02).